# Potential impact of tide-regulation barriers on the formation of methylmercury in the Venice Lagoon (Italy)

Carla Pereira-Garcia, Andrea Bravo, Claudia Cosio, Andrea Gallorini, Simone Leoni, Daniele Cassin, Stéphane Guédron, Thierry Adatte, Miguel Cabrera-Brufau, Olga Sánchez, et al.

Journal of Hazardous Materials 485 (2025) 136747

Contents lists available at ScienceDirect

Journal of Hazardous Materials

journal homepage: www.elsevier.com/locate/jhazmat

# Potential impact of tide-regulation barriers on the formation of methylmercury in the Venice Lagoon (Italy)

Carla Pereira-Garcia [a,*,1], Andrea G. Bravo [a,1,2], Claudia Cosio [b], Andrea Gallorini [c], Simone Leoni [d], Daniele Cassin [d], Stéphane Guédron [e], Thierry Adatte [f], Miguel Cabrera-Brufau [a], Olga Sánchez [g], Silvia G. Acinas [a], David Amouroux [h], Roberto Zonta [d], Janusz Dominik [d], Jean-Luc Loizeau [c]

[a] Departament de Biologia Marina i Oceanografia, Institut de Ciències del Mar, ICM-CSIC, 08003 Barcelona, Catalunya, Spain
[b] Université de Reims Champagne Ardennes, UMR-I 02 INERIS-URCA-ULH SEBIO, Unité Stress Environnementaux et BIOsurveillance des milieux aquatiques, Reims, France
[c] Department F.-A. Forel for Environmental and Aquatic Sciences, and Institute for Environmental Sciences, University of Geneva, Geneva, Switzerland
[d] Istituto di Scienze Marine, Consiglio Nazionale delle Ricerche (ISMAR-CNR), Castello 2737/F, 30122 Venezia, Italy
[e] University of Grenoble Alpes, Univ. Savoie Mont Blanc, CNRS, IRD, IFSTTAR, ISTerre, 38000 Grenoble, France
[f] Institute of Earth Sciences (ISTE), University of Lausanne, 1015 Lausanne, Switzerland
[g] Departament de Genètica i Microbiologia, Facultat de Biociències, Universitat Autònoma de Barcelona, 08193 Bellaterra, Spain
[h] Institut des Sciences Analytiques et de Physico-chimie pour l'Environnement et les Matériaux, CNRS/UNIV Pau & Pays Adour, Pau, France

## HIGHLIGHTS

- MOSE system built to prevent Venice from floods might impact Hg cycle.
- Both MOSE-closing simulations (cold and warm season) had distinct results.
- In the warm season simulation: higher THg, MeHg, DOC and Hg methylation ($k_m$).
- Changes in composition of OM (more labile) correlate to a higher Hg methylation.
- Similar results could be expected after a prolonged real MOSE closing.

## GRAPHICAL ABSTRACT

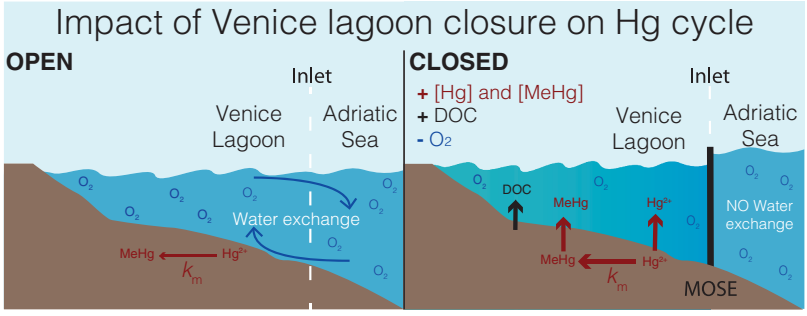


## ARTICLE INFO

*Keywords:*
MeHg formation
Sediments
Temperature
MOSE
Venice Lagoon
Oxygen depletion

## ABSTRACT

Methylmercury (MeHg), a neurotoxic pollutant, is formed mainly under anaerobiosis. The "Modulo Sperimentale Elettromeccanico" (MOSE), built to temporarily close the Venice Lagoon and protect the city from flooding, induces changes in the hydrological regime, reducing water circulation and decreasing in the dissolved oxygen concentrations of the lagoon. Our study shows the potential changes in sediment and overlying water physico-chemistry in a simulated MOSE closing-event by incubating sediment cores for 48 h in the laboratory and deploying benthic chambers. In the incubated summer cores (September 2021), a significant increase in total Hg

* Corresponding author.
*E-mail addresses:* cpereira9876@gmail.com (C. Pereira-Garcia), Andrea.bravo@icm.csic.es (A.G. Bravo), Jean-Luc.Loizeau@unige.ch (J.-L. Loizeau).
[1] These authors have equally contributed to this work
[2] Contributed equally as the corresponding author

https://doi.org/10.1016/j.jhazmat.2024.136747
Received 5 August 2024; Received in revised form 18 November 2024; Accepted 1 December 2024
Available online 3 December 2024

and MeHg concentrations in the water column was observed and associated with an increase in MeHg formation rates – particularly, MeHg formation rates doubled during the simulated MOSE-closing. This increase was associated to a release of dissolved organic carbon and to an enrichment of proteinaceous substances and reactive humic acids in the overlying waters. All these effects were not evident in late autumn (November 2019), when water temperature was 10 °C lower than in September 2021. Our study suggests that hydrological changes caused by the MOSE closure may in some periods increase MeHg concentrations within the Venice Lagoon.

## 1. Introduction

Mercury (Hg) is one of the top ten chemicals of public health concern [1], and particularly its methylated form (methylmercury – MeHg) which has the greatest potential for environmental and human health detriment [2]. MeHg can be bioaccumulated and biomagnified through the aquatic food webs [3,4], making fish consumption the major source of human exposure to Hg. The methylation of inorganic Hg to MeHg occurs mainly under anoxic conditions [5,6] and it is mediated by the activity of anaerobic microorganisms carrying specific genes (*hgcAB*) [7]. Sediments, prone to anoxic conditions, stand out as a favored environment for Hg methylation [8,9,6]. Other factors such as organic matter (OM) concentration and composition also influence Hg methylation in sediments. For example, fresh or autochthonous OM rich in proteins or low molecular mass molecules favor Hg methylation [10-13]. Meanwhile, recalcitrant OM enriched in high molecular mass or aromatic molecules strongly binds Hg, making it less bioavailable and thus reducing Hg methylation rates [11,12,14,15,16].

Coastal areas and coastal lagoons are under increasing human pressure from activities such as port operations and industrial development. Additionally, they are vulnerable to the effects of climate change, including rising sea levels and increased temperature. A rise in sea level between 1 and 10 cm could double the probability of flooding in areas with a narrow range of water levels within a period of five years [17], dramatically affecting coastal areas. These coastal environments have significant economic importance due to fisheries and mariculture activities, and thus is imperative to install or strengthen flood protection to safeguard the coastline and prevent massive population displacement [18]. Current trends show that sea temperature is rising at an accelerated rate due to climate change [19]. Increasing temperature leads to higher consumption of dissolved oxygen (DO) due to the higher bacterial respiration activity [20] and reduced DO solubility in the surface ocean [21], both causing a decline in the DO concentration in the oceans [22], especially in coastal areas [23,24].

An exemplary illustration of the multifaceted challenges these areas confront can be found in the Venice Lagoon, where all these diverse concerns converge with the installation of the high tides protection system, "Modulo Sperimentale Elettromeccanico" (MOSE, *Experimental Electromechanical Module*). The Venice Lagoon has long been recognized as a Hg contaminated area [25-27] with an important MeHg biomagnification [28]. The high tides that submerge Venice are becoming more aggressive and more frequent due to sea level rise and local geodynamics [29-31]. As protection against flooding, the construction of the MOSE began in 2003. These mobile barriers isolate for hours or days the lagoon from the sea, stopping water exchange between them and thus increasing water residence time. Under these new hydrological conditions of the lagoon, the water renewal time is expected to increase as a whole [32] with a potential risk of nutrients and contaminants accumulation in the water column [33]. Increased frequency of high tides and thus longer duration of lagoon closure is expected to result in water stagnation, stratification, and eventually the occurrence of hypoxic or anoxic events in the lagoon [34], favorable for enhanced Hg methylation.

The objective of the present study was to assess the previously unknown potential impact of the lagoon isolation from tides, during MOSE closure, on the Hg mobility and MeHg concentration/production at the sediment-water interface. This study was designed to facilitate the interpretation of changes in methylation and auxiliary variables in relation to initial sediment characteristics (hydrodynamically and seasonally dependent) during core incubation experiments, which simulated MOSE closure conditions. Our study provides new insights into the risks of increased MeHg concentrations in a context of MOSE closing event, when DO depletion events in the lagoon are expected to occur more frequently in some parts of the Venice lagoon.

## 2. Methods

### 2.1. Site of study

The Venice Lagoon (Fig. 1) is the largest wetland system in Italy, and it has been widely described in the literature in terms of functioning and ecosystem characteristics (e.g., [35] - and references therein). The surface area is 550 $km^2$, including mudflats, tidal marshes, islands and a complex network of channels and tidal creeks. The average depth is 1.2 m and shallow water areas account for 75 % of the total surface area, but the depth increases to over 10 m in the main channels. The lagoon has three inlets that connect it to the Adriatic Sea with water residence times ranging from 24 h close to the inlets to 20 days in the more confined areas of the lagoon [32]. Releases from a chlor-alkali plant operating in the industrial area of Porto Marghera emitted Hg into the Venice Lagoon (Fig. 1) during the second half of the 20th century [36], causing this sector of the lagoon to be a high Hg accumulation area [35]. However, Marchese et al., [37] found that Hg contamination in the Venice Lagoon started as early as 1760 and peaked in 1810, long before the Porto Marghera chlor-alkali plant was open. Tides have a strong influence in the complex distribution of Hg and other contaminants along the lagoon and also between the sediment and the water column [38]. More recently, Rosati et al., [39] has model the changes in temporal and spatial distribution Hg species within the lagoon, based on hydrodynamics and sediment dynamics as well as on mercury biogeochemistry. The annual average surface water temperature of the lagoon is 17.6 ºC with a large seasonal variation; the lowest monthly temperatures are recorded in January (7.8 ºC) and the highest in July (26.3 ºC) ([23] - and references therein).

The MOSE system [40] was operated for the first time in October 2020 [41] and with it, the Venice Lagoon has become the first large lagoon in the world with a regulated flow. Up to July 2024, MOSE has been activated 84 times (https://www.mosevenezia.eu/il-mose-in-funzione/), and barrier closures have lasted from a few hours to two days, with a typical closure time of four to five hours [42] mainly in autumn, when flood conditions occur more frequently due to weather-marine forcing factors [43].

### 2.2. Sampling sites

Two shallow sites with different continental influences were selected (Fig. 1): i) Osellino (OS), located very close to the mainland and at about 300 m from the mouth of a freshwater tributary of the lagoon, the Canale Osellino, although not directly affected by the outflow of this watercourse; and ii) San Giuliano (SG), situated at 1.3 km south of the mouth of the Canale Osellino, in a sector with greater water exchange than in OS site and a water depth of 56 cm, compared to 24 cm at OS, as referred to the zero level of the tide gauge for the lagoon. OS site is more confined than SG site, presenting a longer water renewal time, lower

hydrodynamics, and finer sediment grain size with higher organic carbon content [34]. Both sites are located in areas characterized by highest accumulation of Hg (0.71 – 1.66 mg Hg /kg dry sediment) in surface sediments [35]. Additionally, both sites had even higher concentrations of Hg in the deeper sediment layers (data extracted from [35]).

### 2.3. Sampling and core processing

Sampling campaigns were performed in November 2019 and in September 2021. In both periods, seven sediment cores (core number: 6 to 12 in Nov 2019 and 13 to 19 in Sep 2021; Table S1) were collected at each site by a diver driving manually Plexiglas tubes (13.4 cm internal diameter) into the sediment. Cores were collected with 28 cm of overlying water, immediately sealed to avoid contact with atmospheric $O_2$ and carefully transported to the laboratory avoiding resuspension. Three cores from each sampling site were directly processed under an inert atmosphere ($N_2$ - filled glove box) to avoid oxidation of sediment and pore water; these cores ("fresh cores") represent the initial, pre-closing conditions of the lagoon. Prior to core sectioning, 750 mL of overlying water was collected at mid-depth with a peristaltic pump and filtered (Sterivex filter 0.45 μm) for dissolved organic matter characterization and trace element analysis, including total mercury (THg) and MeHg. Then sediment was vertically extruded, and two sediment layers were subsampled, corresponding to 0–2 and 2–4 cm depths. Aliquots of sediment were used for direct determination of water content and grain size. The remaining sediment was centrifuged in metal-free tubes (4000 rpm, for 60 min at 4 °C) to extract porewater. Supernatant was filtered (Sterivex filter 0.45 μm) in the $N_2$-filled glove box and directly fixed with HCl (Ultrex, 0.4 %). The pellets were freeze-dried for organic matter characterization (C and N content, hydrogen (HI) and oxygen (OI) indices), and determination of THg, MeHg, and trace element content.

### 2.4. Simulation of MOSE closing-event: sediment core incubations

Three sediment cores from each site were incubated (i.e. "incubated cores) in a dark room at the lagoon water temperature at the time of collection, i.e., 14 °C in Nov 2019 and 24 °C in Sep 2021, to simulate stagnation of the water column. These cores were capped and sealed to avoid oxygen penetration (see Fig. S1 for details on the experimental set up). After approximately 48 h of incubation, the cores were processed in the glove box as described for "fresh cores". The extra cores (No 12 and 19) from each site were also incubated and used for in-situ profiling with microelectrodes (see Section 2.6.1.).

### 2.5. Benthic chambers

Concurrent with coring, a PVC cylindrical benthic chamber (described in [34]) was deployed at both sites for about 48 h in Sep 2021. Benthic chambers were used to study the processes between sediments and overlying water, to measure the sediment oxygen demand and the changes in overall concentrations on Hg species. The chamber was 30 cm in diameter and 27 cm high, with 6 cm of the chamber driven into the sediment. A multi-parameter water probe (Aquaprobe AP 2000; Aquaread Ltd, England) was placed in the center of the chamber to determine the temperature and DO concentration in the isolated water over time. At the end of the exposure period, water samples were collected from each benthic chamber.

### 2.6. Laboratory analyses

#### 2.6.1. In situ core profiling in September 2021

One core of each site (core 12 and core 19) was used to measure DO and $H_2S$ concentrations and redox potential ($E_H$) along a water-sediment vertical profile, by means of a 500-μm microelectrodes (Unisense®, Denmark). The vertical profiles were measured with a resolution of 500 μm, with double measurement for each point and a conditioning time of 25 s. The profile analysis started from a position such as to intercept both the well-mixed water phase and the diffusive boundary layer (about 5 mm above the surface of the sediment). For each subsequent profile (at 24 and 48 h of incubation), the sensors were moved a few millimeters to avoid insertion into the borehole resulting from the previous analysis.

#### 2.6.2. Sedimentological and geochemical analyses

A complete set of laboratory analysis was performed including water content, particle grain size distribution (Coulter LS-100 analyzer), characterization and quantification of the organic matter (OM) Total Organic Carbon (TOC), hydrogen index (HI) and oxygen index (OI) indexes using Rock-Eval 6 (method described in [44]), mineral carbon (MINC) and total nitrogen (TN, CHN Elemental Analyzer). Please see further details in SI.

#### 2.6.3. Hg, MeHg and trace element analyses

Unless otherwise indicated, THg and MeHg analyses were conducted at the University of Geneva. THg in sediments was analyzed by Cold

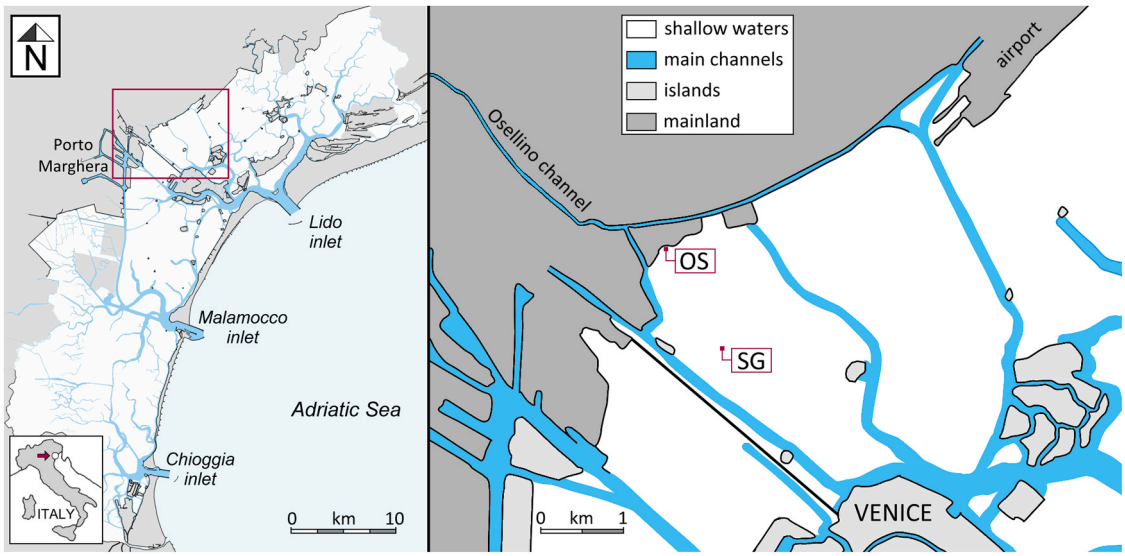


**Fig. 1.** Location of the two studied sites Osellino (OS, 45.4750°, 12.2859°) and San Giuliano (SG, 45.4638°, 12.2949°) in the Venice Lagoon (in the insert).

Vapor Atomic Absorption Spectrophotometry (CVAAS) using a Direct Mercury Analyzer (DMA-80 II, MWS GmbH, Switzerland). All analyses were run in triplicate. The limit of detection (LOD) and working range were 0.01 ng and 0.05 - 600 ng, respectively. The relative error was usually ± 5 % and always less than 10 %. The concentrations obtained for repeated analyses of the certified reference material never exceeded the specified range of concentrations given for SRM 2702 (NIST). THg on water samples was analyzed by Cold Vapor Atomic Fluorescence Spectrometry (CVAFS) (Merx Model III, Brooks Rand, USA) following the EPA Method, revision E 1631 (US-EPA, 2002), with a calculated LOD of 0.06 ng/L and a calculated limit of quantification (LOQ) of 0.2 ng/L. To control the quality of the analysis, two different reference materials were used: ORMS-5 (National Council Research Canada), 26.2 ng/L, which gave a recovery percentage of 88.8 % ± 1.2 %, and a standard solution purchased from Brooks Rand (USA), diluted at 4 ng/L. The percentage of recovery of repeated analyses was between 94.1 % ± 2.5 % and 96.3 % ± 1.3 %. Field and filtration blanks were measured to evaluate the possible contamination during sampling; they reached 0.17 ± 0.04 ng/L in Nov 2019 and 1.0 ± 0.1 ng/L in Sep 2021.

MeHg analysis on sediment were carried out using a $HNO_3$ leaching/$CH_2Cl_2$ extraction method [45]. The certified reference material used in the MeHg analysis (ERM-CC580, European Commission) showed between 91.8 % ± 5.2 % and 98.7 % ± 1.6 % recovery. MeHg analysis on water samples collected in Nov 2019 (overlying water, porewater and water from benthic chambers) was carried out by CVAFS (Merx Model III, Brooks Rand, USA) after distillation following the EPA Method 1630 analysis procedure (US-EPA, 2001), with a calculated LOQ of 0.09 ng/L. To check the accuracy of the analysis we used a spiked sample of a known concentration that showed a recovery efficiency between 89.5 % ± 8.2–96.6 % ± 1.0 %. As this LOQ was close to or higher than the MeHg concentrations observed in some samples, MeHg analyses in pore and overlying waters of samples collected in September 2021 were performed at the University of Grenoble. Filtered MeHg concentrations were analyzed using an ethylation purge and trap-gas chromatograph-AFS analyzer (Tekran® 2700 Methyl Mercury Auto-Analysis System) following published protocols [46,47]. All samples were run in duplicate and quantified using the standard addition technique. The calculated LOQ was 0.02 ng/L.

Mn in water (filtered and acidified with 1 % suprapure $HNO_3$) and in sediments were analyzed using quadrupole-based inductively coupled plasma mass spectrometry (ICP-MS, model 7700 series, Agilent). Sediment digestion was performed in Teflon bombs heated to 150 °C in analytical grade 2 M $HNO_3$ according to the Swiss Soil Protection Ordinance (OSol, OFEV, 1998). The total variation coefficients for triplicate sample measurements were better than 10 %.

#### 2.6.4. Potential Hg methylation rate constants

A slurry, prepared with both sediment layers (0 – 2 cm and 2 - 4 cm) and overlying water, from each core (both fresh and incubated condition), were amended with $^{199}Hg$ (ISC Science, Spain) in a glove box and were either directly frozen (1 aliquot- $t_0$) or incubated in a dark room for 24 h before to be frozen (3 replicates). Determination of Hg transformation rate constants were carried out according to Rodriguez-Gonzalez et al., [48]. These determined rate constants are potential methylation rate constants ($k_m$; Equation 1). Briefly, inorganic Hg and MeHg were extracted from 50 mg of freeze-dried sediments with 5 mL $HNO_3$ (6 N) under focused microwave treatment and analyzed by species specific isotope dilution gas chromatography (GC, Trace GC Thermofisher) hyphenated to an inductively coupled plasma mass spectrometer (ICP-MS, X Series Thermofisher). Methodological detection limits for Hg species were 0.03 ng/g. The extraction and quantification were validated with a CRM (IAEA-405) and recoveries were 102 ± 7 % and 97 ± 4 % for MeHg and inorganic Hg, respectively. The concentration of the formed MeHg deriving from the enriched isotope $^{199}Hg$ was calculated by isotopic pattern deconvolution methodology (Eq1 following [48]).

Equation 1: Potential methylation rate constant. $Me^{199}Hg$ corresponds to the MeHg formed during the incubation time (t; $days^{-1}$)

$$k_m = \frac{\frac{[Me^{199}Hg]}{[Me^{199}Hg]+[I^{199}Hg]}}{t}$$

Calculations of changes in relatives abundances of different Hg stable isotopes and deconvolution have been performed with a developed in-house R package called HgIDAR, available at https://github.com/micro-hg-cpg/HgIDAR.

#### 2.6.5. Fluorescent and Colored Dissolved Organic Matter

The filtered overlying water samples were used for the characterization of optical properties of dissolved organic matter (DOM). Fluorescent and Colored Dissolved Organic Matter (FDOM and CDOM) were measured simultaneously using a Horiba Aqualog spectrofluorometer. Duplicate fluorescence excitation emission matrices (EEMs) were collected for each sample in a 1-cm pathlength quartz cuvette using freshly produced MilliQ water as blank. Fluorescence was recorded from 240 to 600 nm of excitation at 3 nm increments, emission was recorded in the same range (240–600 nm) every 8 pixels (~3 nm) using the instrument CCD detector, and the signal integration time was set to 2 s using the medium gain setting. Absorbance spectra were collected simultaneously to EEMs using the same wavelength range and increments used for EEM excitation.

EMM and absorbance data processing was performed in R using the *staRdom* and *pavo* packages [49,50]. For FDOM processing, MilliQ blank fluorescence was first subtracted and the regions of the EEMs affected by Raman and Rayleigh scatter excluded and values interpolated [51]. Inner filter effects were corrected using the absorbance of each sample [52]. Several FDOM parameters were calculated (Table S2): fluorescence index (FI), humification index (HIX) and biological index (BIX), as well as the common fluorescence peaks A, C, M, T, and B, which were normalized by total fluorescence and are presented as relative abundances [53-56].

### 2.7. Statistical analysis and data visualization

The statistical analyses were performed with R package stats 4.3.2. [57]. Principal Component Analysis (PCA) was used to study the general variability of the sediment samples, and we used the following parameters: MeHg, THg, Hydrogen Index, Oxygen Index, mean diameter of the particles, water content, mineral carbon and the ratio of total organic carbon and total nitrogen. Anova analysis was used to check the differences between conditions, years and sites, for the mentioned variables and the rest of parameters discussed in results and discussion. Visualization was generated with ggplot2 3.4.4. [58] and multi-panels with gridExtra 2.3 [59] of R [57]. The figures were combined and post-processed using Illustrator 24.0.1. The map of the study sites was drawn with CorelDraw.

## 3. Results

### 3.1. Characteristics of the two contrasted sampling sites

#### 3.1.1. Geochemical differences between sampling campaigns and sites

The parameters characterizing the solid phase of studied sediments did not show any significant difference between the two sampled depths (0–2 and 2–4 cm) or among treatments (fresh vs. incubated cores). Thus, the data were combined to compute mean and standard deviation for each site and sampling campaign (n = 12) (Table S3). Moreover, a Principal Component Analysis (PCA, Fig. S2) was performed to explore the differences and similarities between the sediments at the two sites (OS and SG). This analysis resulted in two main components explaining ~66 % of the variability and showing a greater difference between years at SG compared with OS, further details about the differences among

sampling sites and years can be found in supplementary results. In Nov 2019, the dissolved organic carbon (DOC) measured in the overlying water of fresh cores (n = 3) was 2.31 ± 0.13 and 2.37 ± 0.22 mg/L in OS and SG, respectively. In Sep 2021, the DOC was higher at both sites with 4.17 ± 0.02 in OS and 4.07 ± 0.15 mg/L in SG (Table S4).

#### 3.1.2. THg and MeHg concentrations in sediments, and overlying and pore waters in fresh cores

Concentrations of THg in fresh sediments were similar between years and depths but differed across sites, being 0.85 ± 0.05 (n = 12) and 0.93 ± 0.05 (n = 12) mg/kg in OS and SG respectively. Between Nov 2019 and Sep 2021, MeHg levels experienced a notable decline at both sites. In Sep 2021, the values, with a mean of 0.16 ± 0.10 μg/kg, were more than 50 % lower than those recorded in Nov 2019, where the mean was 0.48 ± 0.12 μg/kg.

THg concentrations in porewaters and overlying waters were significantly lower in Nov 2019 compared with Sep 2021 (Table S6) in both sites. In porewaters from Nov 2019, we found THg concentrations ranged from 1.9 to 6.2 ng/L, with the exception of OS 2–4 cm sample that reached 17.1 ng/L. In Sep 2021, THg concentrations in porewaters varied across depths and sites (Figs. 2A and 2C), ranging from 7.7 to 20.4 ng/L and from 8.9 to 23.4 ng/L in OS and SG, respectively. THg concentrations peaked in the 2–4 cm layer, reaching 14.0 ± 5.6 ng/L (n = 3, Sep 2021 in fresh cores) in OS, while in SG they peaked at 0–2 cm, reaching 14.8 ± 7.6 ng/L (n = 3, Sep 2021 in fresh cores). In filtered overlying waters, THg concentrations measured during the 2019 sampling campaign were close or below the detection limits (LOD = 0.06 ng/L), but during the 2021 campaign they increased up to 3.2 ± 0.1 ng/L in OS and 4.4 ± 0.4 ng/L in SG.

### 3.2. Experiments with oxygen limitation: changes in THg, MeHg, $k_m$ and sediment properties

#### 3.2.1. Oxygen, redox and hydrogen sulfide

Sediment cores were incubated to simulate a MOSE-closing event in two different periods (Nov 2019 and Sep 2021). In 2019, at the end of incubation, DO levels at the sediment-water interface dropped to 0.07 and 0.3 mg/L in OS and SG cores, respectively. Concentrations of Mn in the overlying waters did not vary indicating no significant changes in the redox conditions during the 2019 incubations. In contrast, in 2021, relevant changes in DO, redox potential ($E_H$) and $H_2S$ (measured only in OS) profiles were observed after 24 h and 48 h of incubation (Fig. S3). Although both sites had similar DO concentrations (5.12 mg/L) at 5 mm above the sediments, in OS the DO concentrations decreased progressively to a value of 0.4 mg/L at the sediment-water interface, while in SG, DO concentrations were fairly constant but dropped drastically to a value of 1.9 mg/L at the sediment-water interface. In both sites, the DO decreased in overlying waters and sediments after 24 h. The $E_H$ profiles agreed with $O_2$ profiles. In OS, the core reached negative $E_H$ values at ~5 mm depth and decreased progressively with depth to a minimum value at 2 cm depth (Fig. S3). In SG, negative $E_H$ values started at 10 mm depth below the sediment-water interface after 24 h incubation time (−164 mV) and continued decreasing with depth. Concomitant to the decrease in $O_2$ and $E_H$, we observed an important increase of dissolved Mn in the overlying water of OS and SG (Table S7). Lastly, $H_2S$ profiles also concurred with the $E_H$. In OS, $H_2S$ appeared at 5 mm depth and continued increasing with depth and over time (24 h and 48 h, Fig. S3).

#### 3.2.2. THg and MeHg concentrations and Hg methylation rate constants

In Nov 2019, THg and MeHg concentrations did not significantly changed in porewater after 48 h of incubation (Table S6), but this observation should be tempered by the relatively large LOQ on the MeHg analyses. In contrast, in Sep 2021, THg concentrations increased significantly from 3.2 to 10.8 ng/L in the OS overlying waters after 48 h

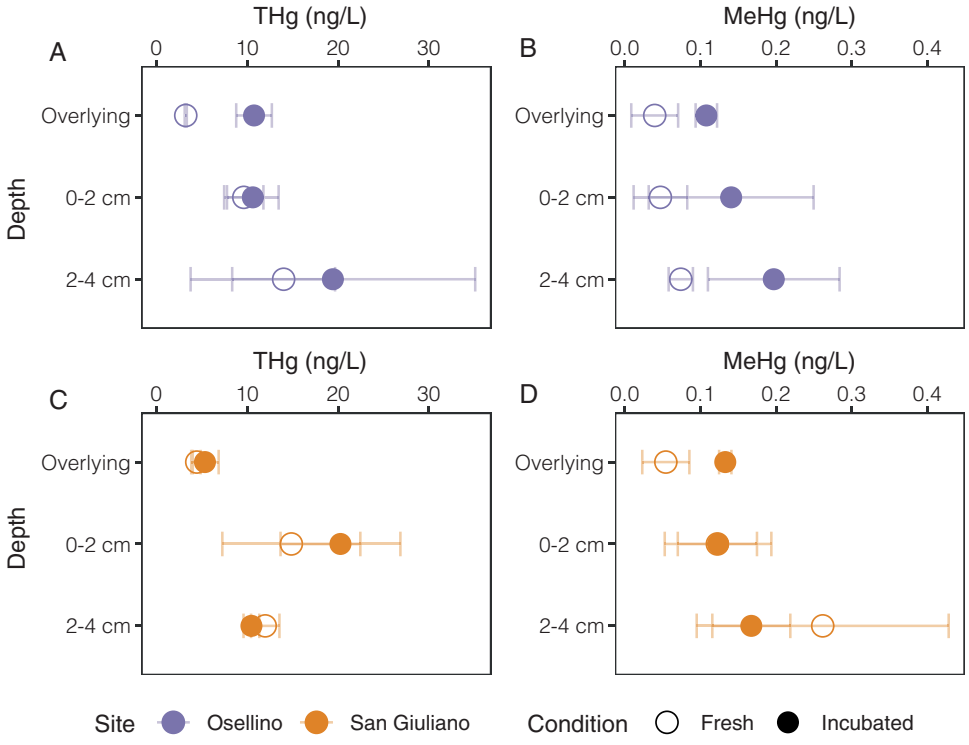


**Fig. 2.** Vertical profiles of THg (A and C) and MeHg (B and D) concentrations in overlying water and porewater of sediment cores from OS site (A and C, purple) and SG site (B and D, orange) collected in Sep 2021. Open symbols represent the measurements performed in fresh cores and closed symbols refer to the incubated cores. Error bars correspond to the standard deviation of environmental triplicates.

of incubation while they remained similar in SG (4.4 and 5.3 ng/L); however, the high variability of replicates makes comparisons difficult. MeHg concentrations rose in both overlying water and porewater of OS after incubation (Fig. 2 and Table S6). In SG, the rise in MeHg concentrations occurred in the overlying waters – reaching approximately the same value as in OS (around 0.1 ng/L, Fig. 2) but remained within the same range in porewater before and after incubation (Fig. 2 and Table S6).

In Nov 2019, differences in potential methylation rate constants ($k_m$; i.e. MeHg formation rate constants) between fresh and incubated cores were not prominent (Figs. 3A and 3C). In contrast, in Sep 2021, $k_m$ almost doubled at both sites after 48 h. Surface sediments (0–2 cm) presented an increase from 0.017 to 0.029 $d^{-1}$ in OS and from 0.009 $d^{-1}$ to 0.017 $d^{-1}$ in SG (Figs. 3B and 3D). In the 2–4 cm sediment layer, a similar trend was observed, with a smaller increase compared to surface sediments.

### 3.2.3. DOC content and DOM properties in overlying water

In Nov 2019, no significant changes in the concentration of dissolved organic carbon (DOC) or the composition of the dissolved organic matter (DOM) were found after incubation of the sediment cores (Table S4). By contrast, in Sep 2021, DOC in the overlying waters of OS increased significantly from 4.2 mg/L to 10.6 mg/L during the incubation (Fig. 4A and Table S4). A smaller increase in DOC from 4.1 to 6.0 mg/L was also observed in SG (Fig. 4A and Table S4).

Regarding the optical properties of DOM in the overlying water, different DOM fluorescent peaks showed changes during the 2021 incubations (Fig. 4). Humic peak A and marine peak M decreased significantly after incubation in OS overlying water. Humic peak C remained unchanged after incubation. In contrast, a different trend was observed in SG, as peaks A, C and M were not affected by the incubation (Fig. 4 and Table S4). Both sites, and especially OS, presented a smaller A/C peak ratio after incubation (Fig. 4B). An increase in the C/M ratio was also observed (Table S4). Peaks T and B, associated to tryptophane and tyrosine respectively, increased in overlying waters during the incubation in both sites (Fig. 4F and Table S4). The T/C ratio, used as a proxy of the proportion of proteinaceous substances (often more available for bacteria) over the humic substances, also increased during the incubation, with a greater increase in OS than in SG (Fig. 4C).

The protein related components might be explained by either the release from the sediments or the formation due to a higher microbial activity. Peak A represents general terrestrial humics, while peak C represents a more degraded humic component. The decrease in the A/C ratio thus indicates a change in humic composition towards the dominance of more degraded substances. Taken together DOC and optical properties of DOM, our results hint towards a release of organic matter from the sediments to the overlying waters, with an associated enrichment in labile/available substances (more proteinaceous), and a higher proportion of reactive humic substances (decrease in A/C ratio). All likely promoting MeHg formation in surface sediments and potentially in the overlying waters.

### 3.3. Changes in THg and MeHg in benthic chambers

In Sep 2021, benthic chambers were deployed at OS and SG to measure in situ DO consumption and to complement the incubations performed in laboratory conditions. The confined overlying water reached total anoxia after 11 and 18 h in OS and SG, respectively (Fig. 5). After 48 h, concentrations of THg, MeHg and DOC and organic matter composition were measured in the overlying water. THg concentrations were 13.5 ng/L in OS and 10.4 ng/L in SG (Table S8). The increment in OS is comparable to the one observed in the overlying

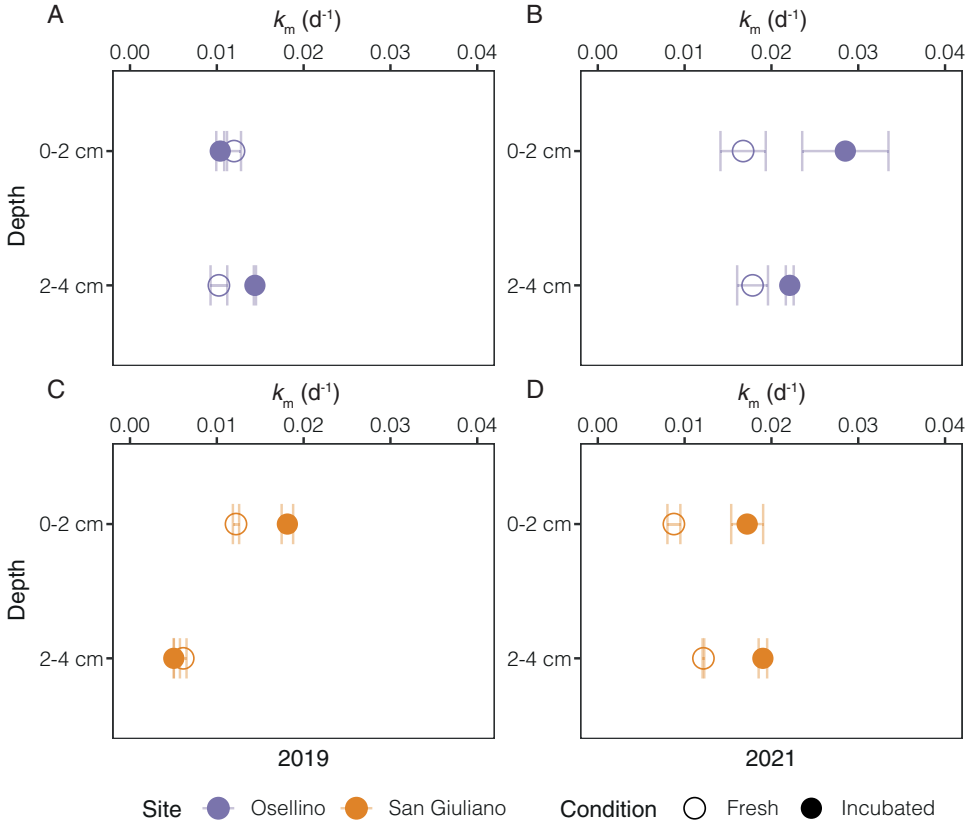


**Fig. 3.** Potential Hg methylation rate constants ($k_m$, $d^{-1}$) determined in both sites (OS in purple and SG in orange) during the 2019 and 2021 incubations. Panels A and C correspond to Nov 2019, while B and D to Sep 2021; open and close symbols refer to fresh and incubated cores respectively. Error bars correspond to the standard deviation of the three environmental replicates.

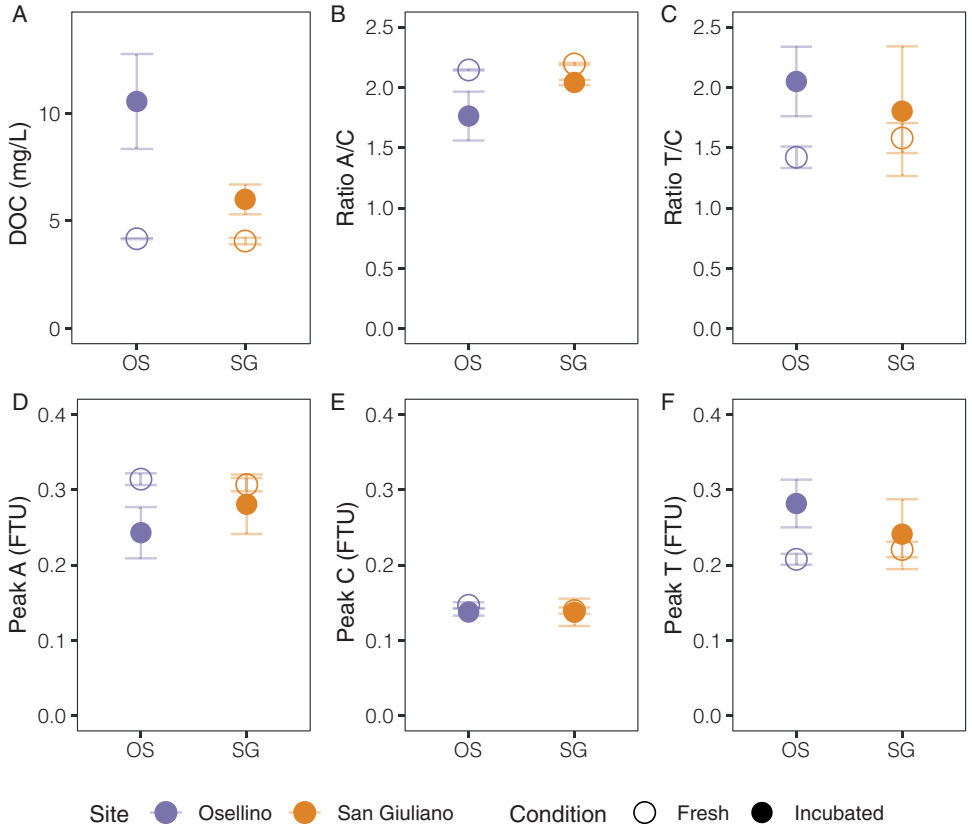


**Fig. 4.** DOC and fluorescent dissolved organic matter (FDOM) characterization of the overlying water collected in the Sep 2021 sampling campaign. Values of fresh (open symbols) and incubated cores (close symbols) from both sites (OS in purple and SG in orange). Peaks A, C and T are normalized by total fluorescence.

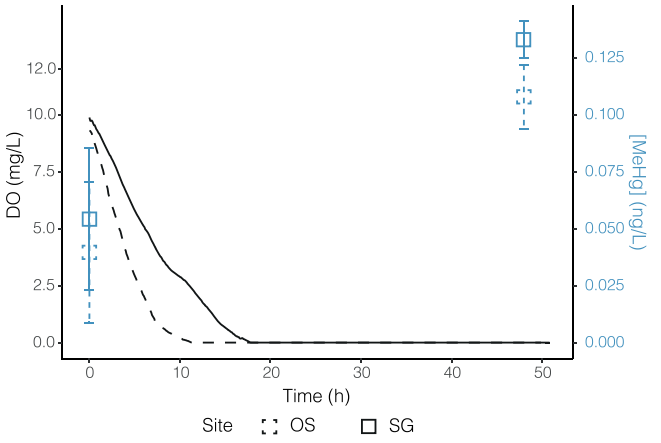


**Fig. 5.** Conceptual figure coupling the consumption of dissolved oxygen (DO, lines) in benthic chambers in Sep 2021 with the simultaneous increase in methylmercury concentration (MeHg, squares) in the overlying waters of fresh ($t_0$) and incubated cores (48 h).

water of the sediment cores during the incubation (THg concentrations increased from 3.2 to 10.7 ng/L, Fig. 2). In the SG benthic chamber, however, THg concentrations were higher compared to those in the cores (4.4 ng/L in fresh cores and 5.3 ng/L in incubated cores, Fig. 2). In benthic chambers, MeHg concentrations after 48 h were 0.07 ng/L in OS and 0.13 ng/L in SG (Table S8). These MeHg concentrations are similar to those measured in incubated cores (0.11 and 0.13 ng/L in OS and SG respectively, Fig. 2), although a lower MeHg concentration was observed in the OS benthic chambers than in the incubated cores. Both DOC content and DOM composition of the benthic chambers were similar to the values found in the fresh cores of the experiments (Table S7). Additionally, Mn, that is released from the sediment to the overlying water when $E_H$ decreases, increased during benthic camber deployment from 28.5 to 216 μg/L and from 7.4 to 115 μg/L in OS and SG respectively, as observed in incubated sediment cores.

## 4. Discussion

### 4.1. Contrasting study sites

The PCA analysis shows that sediments from OS in both sampling years and from SG in Nov 2019 are very similar with respect to the analyzed sedimentological characteristics (grain size and organic matter content and composition). Surface sediments from SG in Sep 2021 are different, with lower water and OM content, higher TOC/N and lower HI which is indicative of a less degraded OM [60,61]. Additional observations of sediment cores (CT image, trace element profiles – not shown) strongly suggests more dynamic sedimentary conditions at site SG, which, furthermore, is located in an area with a greater probability of sediment disturbance by anthropogenic activities. Changes in sediment characteristics at the same site (grain-size, OM and MINC) on an yearly scale are not unusual as observed by Guédron et al. [38] in the northern part of the lagoon. Sediment heterogeneity at site SG estimated by the variability coefficient of the auxiliary variables was clearly higher than at the OS site in both sampling periods. However, the heterogeneity at the SG site was not higher in Sep 2021 than in Nov 2019, except for mean grain-size which is driven by a larger proportion of particles of 16 μm in core SG17 at 2–4 layer. If this sample is not considered, grain size distribution does not change between years.

THg concentrations in sediments at both sites, ranging between 0.72 and 1.08 mg/kg, are lower than those measured in 2008 (1.66 mg/kg in the 5 upper cm) in the vicinity of Osellino canal [35]. In the overlying

and pore waters, the differences in THg concentrations between sampling campaigns could be a result of the tide phase. In Nov 2019, the samples were taken during an ebb tide, while in Sep 2021, they were collected during a flood tide. This interpretation agrees with the results of Guédron et al. [38], who observed the highest concentrations of THg during the rising tide in the northern part of the lagoon.

### 4.2. Increase in methylmercury formation and concentration in a simulated MOSE closing-event

Our experiment in Sep 2021 consistently showed an increase in MeHg concentrations in overlying waters after both simulations of the MOSE closing-event: benthic chambers (Table S8) and incubation of sediment cores (Figs. 2C and 2D). This increase in MeHg concentrations was associated with oxygen depletion (Fig. 5) and a decrease in $E_H$ (Fig. S3). Decreases in $E_H$ have been associated with a release of DOC and an enrichment of humic substances in porewaters, especially under sulfate-reducing conditions [62]. Indeed, Hg is strongly bound to sulfur sites of organic matter, in particular humic acids [63] and, as a consequence, positive correlations between THg and DOC concentrations have often been reported in aquatic systems [11,64,15,65,66] and in our experiments (Fig. 6, r = 0.96, p-value < 0.001). In our incubations, DOC concentrations in overlying waters doubled and reached up to ~ 6 and 10 mg/L in SG and OS, respectively. A previous study conducted under laboratory conditions, showed that an increase in DOC led to a raise in Hg-availability until ~ 11 mg/L and then to a decline at higher DOC concentrations [12]. The increase of DOC could have thus similarly increased Hg availability during the simulated MOSE-closing event. Moreover, we observed in the incubated samples a decrease of humic peak A but also of the A/C peak ratio (Fig. 4 and Table S7), indicating an enrichment in degraded humic compounds which could result from an intense sulfate reduction [62]. Indeed, the A/C ratio correlated negatively with the $k_m$ (r = −0.66 and p-value = $1.8 \times 10^{-5}$, Fig. 6). After 48 h, we also observed an enrichment in labile protein-like substances (peak T, Fig. 4), generally produced by the activity of bacteria and phytoplankton [53,67,68] and was positively correlated to the $k_m$ measured in surface sediments (Fig. 6, r = 0.63 and p-value = 0.05).

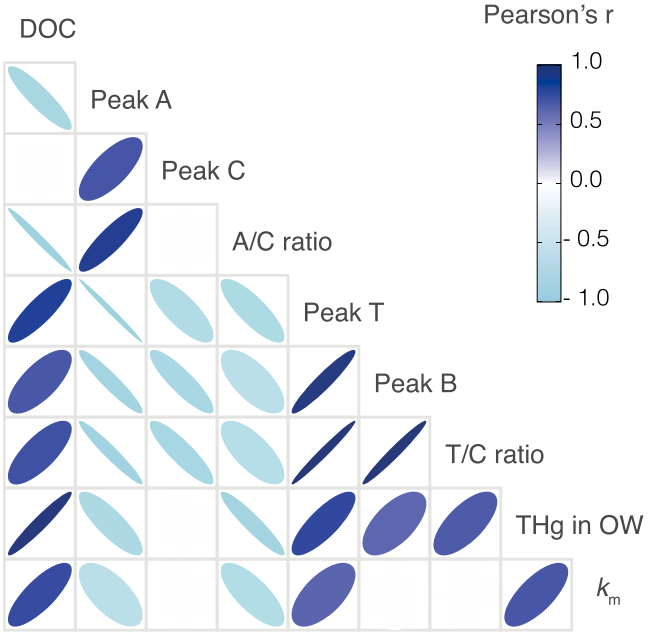


**Fig. 6.** Pearson correlation matrix between $k_m$, Hg and MeHg concentrations and organic matter composition. Data from both fresh and incubated cores from Sep 2021 sampling were used to construct the Pearson correlation matrix. Only significant (p < 0.05) correlations are shown.

Taking all this into consideration, it is plausible that the increase in MeHg concentrations in overlying waters observed in this study resulted from an enhanced Hg methylation (Fig. 3), fostered by the release of available Hg, associated to the increase in DOC [11,12,16], and labile dissolved organic matter (peak T) (Fig. 4) [15]. The low oxygen concentrations found in the studied sediments together with an enrichment in labile dissolved organic matter have been associated to a higher presence of Hg methylating microorganisms [69].

Noteworthy to mention that Hg methylation and MeHg demethylation after 48 h incubation have likely reached a steady state [48,70] and we can assume that measured potential methylation reflect the net MeHg formation in sediment. Hg methylation rate constants measured in this study were higher than pristine coastal sediments such as those of the Gulf of Trieste [71], but ranged within the known limits for the Venice Lagoon described in previous studies [38,72] and other urban coastal areas [70,73]. Bouchet et al. [70] also measured higher values of $k_m$ during the warmer season in the Arcachon Bay (France).

The observed increase in MeHg concentrations in the overlying and porewater in our experiments of Sep 2021 could impact MeHg biomagnification because filter-feeding benthic bivalves have been identified as key organisms in the transfer of MeHg from sediments to higher levels of the food chain in the Venice Lagoon [25,28] and in other Mediterranean lagoons, like Grado and Marano [74]. Furthermore, the bioavailability of Hg might have increased at the measured DOC concentrations and thus could lead to enhanced Hg accumulation in food webs [75].

According to a current estimate of the Hg budget [27], sediments remain the main source of Hg to the lagoon water. Although surface sediment layers lose Hg by burial and export to the Adriatic Sea, Hg inventory is high enough to support considerable MeHg formation for decades. Potentially, increasing MeHg formation may compensate for decreasing Hg inventory.

The experimental design in this study attempt to replicate the conditions of a long MOSE closing event, but both approaches, benthic chambers and sediment core incubations, have limitations. The complexity of the natural environment is too large to completely replicate experimental conditions. Both methodologies isolate completely the sample, which would not happen as drastically in reality as the lagoon has its own internal currents and exchanges. Additionally, temperature seems to play an important role in the interpretation of the results; temperature remained constant in the experiments however in a real long lasting event of the MOSE, the temperature would shift along the day.

### 4.3. Negative consequences of oxygen depletion events on coastal Hg cycling

Temperature is one of the key factors to consider in the current situation of the Venice Lagoon. To study the potential impact of MOSE closing-events in different times of the year, we performed the same experiment in different seasons. In 2019, we collected the sediments in November, and incubated them at the water temperature (14 °C) simulating the autumn conditions. In 2021, we collected the cores in September and incubated them at 24 °C, simulating the end of summer conditions. These differences in setup helped us to understand what could potentially happen if the MOSE closes when temperatures are higher, either because closure occurs earlier in the year with respect to the present situation or because temperatures increase during the fall due to climate change. By choosing different seasons we took into account not only temperature differences, but also potentially different types of OM in surface sediments. During the Nov 2019 campaign, we did not observe any significant changes in the concentration or composition of organic matter or in $k_m$ after incubation. In contrast, the results of the Sep 2021 campaign showed a different outcome. In Nov 2019, there was still some DO in the water after 45 h, whereas in Sep 2021 there was no DO after only 11 h or 18 h (OS and SG respectively)

(Fig. 5). Although we measured similar DO concentrations at both sites at the beginning of the experiment in 2021, we detected a faster reduction of DO in OS than in SG. A considerably lower sediment oxygen demand (SOD) throughout the year was measured at sites close to SG than near OS [34]. This may explain a lower $k_m$ at SG compared to OS not only in September, but also during all warm months. Moreover, the increase in protein-like substances suggests a higher bacterial activity. This effect was more pronounced in OS and helps to explain the faster decrease in DO. Higher bacterial activity, less DO and an enrichment of proteinaceous OM, potentially caused by MOSE-closing events, are important drivers for Hg methylation [11]. However, the differences observed between SG and OS highlights that the impact of MOSE-closing events may not be homogeneous across the lagoon, and that further studies are required to better constrain and predict the effects of MOSE in the increase in MeHg concentration in the entire lagoon.

As a consequence of rising temperatures, the sea level increases [30, 40], a fact that has been observed in the Venice Lagoon, where the number of flooding events have doubled in the last decade (2010s) [30]. Currently, the MOSE normally closes for short periods of time and during cold months of the year, minimizing the impact of the MOSE on the sediment oxygen demand [34] but the ongoing global change could modify the situation, in fact during the summer of 2023 the MOSE had to close three times. As sea temperature rises [19,23], the SOD will start to increase, more rapidly in confined areas (such as OS) where unusually high values of SOD were already found [34]. At the same time, higher temperature might lead to a decline in oxygen solubility [21] and enhanced bacterial activity [20], also favoring MeHg formation in the lagoon.

Overall, our study shows that the difference in MeHg formation and MeHg concentrations found after incubation would be intensified by the rising temperature and this may result in periods of MeHg formation as the MOSE closes more often and for longer periods. As well, a larger increase of MeHg formation in marginal sites such as OS during a MOSE closing event, may act as a hot spot for MeHg formation followed by redistributed across the lagoon during the tidal cycling [38] and potentially enter the food web. Considering Rova et al. [76] demonstrated that the seafood resources are abundant in the confined waters of the lagoon and partly in open water borders, including San Giuliano area, where an increased production and release of MeHg can be expected during prolonged isolation of the lagoon from the Adriatic, this should be considered in future monitoring strategies.

## 5. Conclusions

The MOSE was built to isolate temporarily the Venice Lagoon from the Adriatic Sea during high tide events and protect the city of Venice and its cultural heritage from flooding. In this study, we simulated the potential effect of a prolonged MOSE-closing event and showed that MeHg concentrations increased in porewaters and overlying waters as a result of an enhanced MeHg formation caused by a release of labile DOC. This increase might have a relevant impact on MeHg accumulation in the Venice Lagoon biota. The incubation experiments cannot reproduce all of the conditions occurring during a real MOSE closure event and might have created more extreme isolation conditions. Nevertheless, in the context of global change, with rising temperatures and declining oxygen concentrations in coastal areas prone to MeHg methylation, our study highlights the need to monitor the MeHg concentrations after activation of the MOSE system, especially during warm months. Low water temperatures did not foster a relevant DO consumption and therefore did not enhance MeHg formation but long-lasting MOSE closure at higher temperatures in the future may lead to an increase in MeHg concentrations in water and food webs of the Venice Lagoon.

## Environmental implication

Coastal areas are experiencing the consequences of global change (oxygen depletion, rising temperatures, direr floods…). We focused on the Venice Lagoon to assess the changes in MeHg formation under a tide-regulation system (MOSE). The MOSE is needed to prevent flooding, but the consequences of its operation (e.g. higher MeHg formation) could be critical for the lagoon's environmental health. The increase in MeHg concentrations within the lagoon is specially concerning, since it might lead to an increase of MeHg in biota, especially during warm seasons. This study features the importance of investigations under actual MOSE-closing events and similar coastal ecosystems.

## Funding

This work is part of the Research Programme Venezia 2021 (Scientific research program for a "regulated" lagoon), coordinated by CORILA (Consortium for coordination of research activities concerning the Venice Lagoon system), and funded by the Ministero delle Infrastrutture e dei Trasporti (Provveditorato Interregionale per le Opere Pubbliche del Veneto - Tren-tino Alto Adige - Friuli Venezia Giulia), grant number 21/18/AC_AR02 (04/12/2018). Andrea G. Bravo acknowledges Ramon y Cajal Program (RYC2019-028400). The PhD of Carla Pereira-García was funded by the project MER-CLUB (project MER-CLUB, 863584-MER_CLUB-EMFF-BlueEconomy-2018) to Silvia G. Acinas and Olga Sánchez and by the Marie Curie Individual Fellowship (H2020-MSCA-IF-2016; project-749645) of Andrea G. Bravo. Miguel Cabrera-Brufau was supported by a predoctoral grant from the Spanish Government (FPU16-01925) and the research group "Plankton Ecology and Ocean Health" (2021 SGR 0047). This study acknowledges the "Severo Ochoa Centre of Excellence" accreditation (CEX2019-000298-S) to the ICM.

## CRediT authorship contribution statement

**Miguel Cabrera-Brufau:** Writing – review & editing, Investigation, Formal analysis, Data curation. **Thierry Adatte:** Writing – review & editing, Investigation, Formal analysis, Data curation. **Stéphane Guédron:** Writing – review & editing, Investigation, Formal analysis. **Daniele Cassin:** Writing – review & editing, Investigation, Formal analysis. **Simone Leoni:** Writing – review & editing, Investigation, Formal analysis, Data curation. **Jean-Luc Loizeau:** Writing – review & editing, Resources, Project administration, Methodology, Investigation, Funding acquisition, Formal analysis, Conceptualization. **Andrea Gallorini:** Writing – review & editing, Investigation, Formal analysis, Data curation. **Janusz Dominik:** Writing – review & editing, Methodology, Investigation, Formal analysis, Conceptualization. **Claudia Cosio:** Writing – review & editing, Investigation. **Roberto Zonta:** Writing – review & editing, Resources, Project administration, Methodology, Investigation, Funding acquisition, Formal analysis, Conceptualization. **Andrea G. Bravo:** Writing – review & editing, Writing – original draft, Supervision, Project administration, Methodology, Investigation, Funding acquisition, Data curation, Conceptualization. **David Amouroux:** Writing – review & editing, Resources. **Carla Pereira-Garcia:** Writing – review & editing, Writing – original draft, Visualization, Software, Investigation, Formal analysis, Data curation. **Silvia G. Acinas:** Writing – review & editing, Supervision. **Olga Sánchez:** Writing – review & editing, Supervision.

## Declaration of Competing Interest

The authors declare that they have no known competing financial interests or personal relationships that could have appeared to influence the work reported in this paper.

## Acknowledgments

We would like to thank Daniele Curiel (SELC, Venice) for underwater sampling and Loris Dametto and Giorgia Manfè (ISMAR CNR) for the support in the field activity, and Philippe Arpagaus, Killian Kavanagh,

Aurora Pinto (University of Geneva) for their help in the laboratory. We extend our thanks to Dr. Bastien Duval and Dr. Emmanuel Tessier for their invaluable contributions to the training of Carla Pereira-García.

## Appendix A. Supporting information

Supplementary data associated with this article can be found in the online version at doi:10.1016/j.jhazmat.2024.136747.

## Data Availability

Data will be made available on request.

## References

[1] World Health Organization. (2020). The 10 chemicals of major public health concerns. ⟨https://www.who.int/teams/environment-climate-change-and-health/chemical-safety-and-health/health-impacts/chemicals⟩.
[2] Clarkson, T.W., Magos, L., 2006. The toxicology of mercury and its chemical compounds. Crit Rev Toxicol 36 (8), 609–662. https://doi.org/10.1080/10408440600845619.
[3] Mason, R.P., Reinfelder, J.R., Morel, F.M.M., 1995. Bioaccumulation of mercury and methylmercury. Water Air Soil Pollut 80 (1), 915–921. https://doi.org/10.1007/BF01189744.
[4] Mason, R.P., Reinfelder, J.R., Morel, F.M.M., 1996. Uptake, toxicity, and trophic transfer of mercury in a coastal diatom. Environ Sci Technol 30 (6), 1835–1845. https://doi.org/10.1021/es950373d.
[5] Eckley, C.S., Hintelmann, H., 2006. Determination of mercury methylation potentials in the water column of lakes across Canada. Sci Total Environ 368 (1), 111–125. https://doi.org/10.1016/j.scitotenv.2005.09.042.
[6] Pak, K.-R., Bartha, R., 1998. Mercury methylation and demethylation in anoxic lake sediments and by strictly anaerobic bacteria. Appl Environ Microbiol 64 (3), 1013–1017. https://doi.org/10.1128/AEM.64.3.1013-1017.1998.
[7] Parks, J.M., Johs, A., Podar, M., Bridou, R., Hurt, R.A., Smith, S.D., et al., 2013. The genetic basis for bacterial mercury methylation. Science 339 (6125), 1332–1335. https://doi.org/10.1126/science.1230667.
[8] Bravo, A.G., Bouchet, S., Guédron, S., Amouroux, D., Dominik, J., Zopfi, J., 2015. High methylmercury production under ferruginous conditions in sediments impacted by sewage treatment plant discharges. Water Res 80, 245–255. https://doi.org/10.1016/j.watres.2015.04.039.
[9] Hines, M.E., Poitras, E.N., Covelli, S., Faganeli, J., Emili, A., Žižek, S., et al., 2012. Mercury methylation and demethylation in Hg-contaminated lagoon sediments (Marano and Grado Lagoon, Italy). Estuar Coast Shelf Sci 113, 85–95. https://doi.org/10.1016/j.ecss.2011.12.021.
[10] Bouchet, S., Goñi-Urriza, M., Monperrus, M., Guyoneaud, R., Fernandez, P., Heredia, C., et al., 2018. Linking microbial activities and low-molecular-weight thiols to Hg methylation in biofilms and periphyton from high-altitude tropical lakes in the bolivian altiplano. Environ Sci Technol 52 (17). https://doi.org/10.1021/acs.est.8b01885.
[11] Bravo, A.G., Bouchet, S., Tolu, J., Björn, E., Mateos-Rivera, A., Bertilsson, S., 2017. Molecular composition of organic matter controls methylmercury formation in boreal lakes. Nat Commun 8 (1), 14255. https://doi.org/10.1038/ncomms14255.
[12] Chiasson-Gould, S.A., Blais, J.M., Poulain, A.J., 2014. Dissolved organic matter kinetically controls mercury bioavailability to bacteria. Environ Sci Technol 48 (6), 3153–3161. https://doi.org/10.1021/es4038484.
[13] Schaefer, J.K., Szczuka, A., Morel, F.M.M., 2014. Effect of divalent metals on Hg(II) uptake and methylation by bacteria. Environ Sci Technol 48 (5), 3007–3013. https://doi.org/10.1021/es405215v.
[14] Graham, A.M., Aiken, G.R., Gilmour, C.C., 2013. Effect of dissolved organic matter source and character on microbial Hg methylation in Hg–S–DOM solutions. Environ Sci Technol 47 (11), 5746–5754. https://doi.org/10.1021/es400414a.
[15] Herrero Ortega, S., Catalán, N., Björn, E., Gröntoft, H., Hilmarsson, T.G., Bertilsson, S., et al., 2018. High methylmercury formation in ponds fueled by fresh humic and algal derived organic matter: high methylmercury formation in ponds. Limnol Oceanogr 63 (S1), S44–S53. https://doi.org/10.1002/lno.10722.
[16] Soerensen, A.L., Schartup, A.T., Skrobonja, A., Björn, E., 2017. Organic matter drives high interannual variability in methylmercury concentrations in a subarctic coastal sea. Environ Pollut 229, 531–538. https://doi.org/10.1016/j.envpol.2017.06.008.
[17] Taherkhani, M., Vitousek, S., Barnard, P.L., Frazer, N., Anderson, T.R., Fletcher, C. H., 2020. Sea-level rise exponentially increases coastal flood frequency. Sci Rep 10 (1), 6466. https://doi.org/10.1038/s41598-020-62188-4.
[18] Vousdoukas, M.I., Mentaschi, L., Voukouvalas, E., Bianchi, A., Dottori, F., Feyen, L., 2018. Climatic and socioeconomic controls of future coastal flood risk in Europe. Nat Clim Change 8 (9), 776–780. https://doi.org/10.1038/s41558-018-0260-4.
[19] Cheng, L., Abraham, J., Hausfather, Z., Trenberth, K.E., 2019. How fast are the oceans warming? Science 363 (6423), 128–129. https://doi.org/10.1126/science.aav7619.
[20] Nydahl, A., Panigrahi, S., Wikner, J., 2013. Increased microbial activity in a warmer and wetter climate enhances the risk of coastal hypoxia. FEMS Microbiol Ecol 85 (2), 338–347. https://doi.org/10.1111/1574-6941.12123.
[21] Schmidtko, S., Stramma, L., Visbeck, M., 2017. Decline in global oceanic oxygen content during the past five decades. Nature 542 (7641), 335–339. https://doi.org/10.1038/nature21399.
[22] Breitburg, D., Levin, L.A., Oschlies, A., Grégoire, M., Chavez, F.P., Conley, D.J., et al., 2018. Declining oxygen in the global ocean and coastal waters. Science 359 (6371), eaam7240. https://doi.org/10.1126/science.aam7240.
[23] Amos, C.L., Umgiesser, G., Ghezzo, M., Kassem, H., Ferrarin, C., 2017. Sea surface temperature trends in Venice Lagoon and the adjacent waters. J Coast Res 332, 385–395. https://doi.org/10.2112/JCOASTRES-D-16-00017.1.
[24] Pitcher, G.C., Aguirre-Velarde, A., Breitburg, D., Cardich, J., Carstensen, J., Conley, D.J., et al., 2021. System controls of coastal and open ocean oxygen depletion. Prog Oceanogr 197, 102613. https://doi.org/10.1016/j.pocean.2021.102613.
[25] Bloom, N.S., Moretto, L.M., Ugo, P., 2004. A comparison of the speciation and fate of mercury in two contaminated coastal marine ecosystems: The Venice Lagoon (Italy) and Lavaca Bay (Texas). Limnol Oceanogr 49 (2), 367–375. https://doi.org/10.4319/lo.2004.49.2.0367.
[26] Pavoni, B., Marcomini, A., Sfriso, A., Donazzolo, R., Orio, A.A., 1992. Changes in an estuarine ecosystem. In: The Science of Global Change, 483. American Chemical Society, pp. 287–305. https://doi.org/10.1021/bk-1992-0483.ch014.
[27] Rosati, G., Solidoro, C., Canu, D., 2020. Mercury dynamics in a changing coastal area over industrial and postindustrial phases: lessons from the Venice Lagoon. Sci Total Environ 743, 140586. https://doi.org/10.1016/j.scitotenv.2020.140586.
[28] Dominik, J., Tagliapietra, D., Bravo, A.G., Sigovini, M., Spangenberg, J.E., Amouroux, D., et al., 2014. Mercury in the food chain of the Lagoon of Venice, Italy. Mar Pollut Bull 88 (1-2), 194–206. https://doi.org/10.1016/j.marpolbul.2014.09.005.
[29] Lionello, P., 2012. The climate of the venetian and north Adriatic region: variability, trends and future change. Phys Chem Earth Parts A/B/C 40-41, 1–8. https://doi.org/10.1016/j.pce.2012.02.002.
[30] Lionello, P., Nicholls, R.J., Umgiesser, G., Zanchettin, D., 2021. Venice flooding and sea level: Past evolution, present issues, and future projections (introduction to the special issue). Nat Hazards Earth Syst Sci 21 (8), 2633–2641. https://doi.org/10.5194/nhess-21-2633-2021.
[31] Scarascia, L., Lionello, P., 2013. Global and regional factors contributing to the past and future sea level rise in the Northern Adriatic Sea. Glob Planet Change 106, 51–63. https://doi.org/10.1016/j.gloplacha.2013.03.004.
[32] Ferrarin, C., Ghezzo, M., Umgiesser, G., Tagliapietra, D., Camatti, E., Zaggia, L., et al., 2013. Assessing hydrological effects of human interventions on coastal systems: numerical applications to the Venice Lagoon. Hydrol Earth Syst Sci 17 (5), 1733–1748. https://doi.org/10.5194/hess-17-1733-2013.
[33] National Research Council, 2000. What determines susceptibility to nutrient over-enrichment? En Clean Coastal Waters: Understanding and Reducing the Effects of Nutrient Pollution. The National Academies Press, Washington, DC. https://doi.org/10.17226/9812.
[34] Leoni, S., Dominik, J., Cassin, D., Manfè, G., Tagliapietra, D., Acri, F., et al., 2022. Sediment oxygen demand rate in a flow regulated lagoon (Venice, Italy). Front Environ Sci 10, 1000665. https://doi.org/10.3389/fenvs.2022.1000665.
[35] Zonta, R., Botter, M., Cassin, D., Bellucci, L.G., Pini, R., Dominik, J., 2018. Sediment texture and metal contamination in the Venice Lagoon (Italy): a snapshot before the installation of the MOSE system. Estuar Coast Shelf Sci 205, 131–151. https://doi.org/10.1016/j.ecss.2018.03.007.
[36] Zonta, R., Botter, M., Cassin, D., Pini, R., Scattolin, M., Zaggia, L., 2007. Sediment chemical contamination of a shallow water area close to the industrial zone of Porto Marghera (Venice Lagoon, Italy). Mar Pollut Bull 55 (10-12), 529–542. https://doi.org/10.1016/j.marpolbul.2007.09.024.
[37] Marchese, E., Bizzotto, E.C., Giubilato, E., Semenzin, E., Marcomini, A., 2022. Pre-industrial sediment concentrations of metals: insights from the Venice lagoon (Italy). Environ Sci Pollut Res 29 (57), 85829–85838. https://doi.org/10.1007/s11356-022-23378-x.
[38] Guédron, S., Huguet, L., Vignati, D.A.L., Liu, B., Gimbert, F., Ferrari, B.J.D., et al., 2012. Tidal cycling of mercury and methylmercury between sediments and water column in the Venice Lagoon (Italy). Mar Chem 130, 1–11. https://doi.org/10.1016/j.marchem.2011.12.003.
[39] Rosati, G., Solidoro, C., Laurent, C., Alcázar, L.A., Umgiesser, G., Canu, D., 2024. Mercury cycling in contaminated coastal environments: modeling the benthic-pelagic coupling and microbial resistance in the Venice Lagoon. Water Res 261, 121965. https://doi.org/10.1016/j.watres.2024.121965.
[40] Trincardi, F., Barbanti, A., Bastianini, M., Benetazzo, A., Cavaleri, L., Chiggiato, J., et al., 2016. The 1966 flooding of Venice: What time taught us for the future. Oceanography 29 (4). https://doi.org/10.5670/oceanog.2016.87.
[41] Mel, R.A., Viero, D.P., Carniello, L., Defina, A., D'Alpaos, L., 2021. The first operations of Mo.S.E. system to prevent the flooding of Venice: insights on the hydrodynamics of a regulated lagoon. Estuar, Coast Shelf Sci 261, 107547. https://doi.org/10.1016/j.ecss.2021.107547.
[42] Alberti, T., Anzidei, M., Faranda, D., Vecchio, A., Favaro, M., Papa, A., 2023. Dynamical diagnostic of extreme events in Venice lagoon and their mitigation with the MoSE. Sci Rep 13 (1), 10475. https://doi.org/10.1038/s41598-023-36816-8.
[43] Camuffo, D., 1993. Analysis of the sea surges at Venice from A.D. 782 to 1990. Theor Appl Climatol 47 (1), 1–14. https://doi.org/10.1007/BF00868891.
[44] Behar, F., Beaumont, V., De, B., Penteado, H.L., 2001. Rock-Eval 6 technology: performances and developments. Oil Gas Sci Technol 56 (2), 111–134. https://doi.org/10.2516/ogst:2001013.
[45] Bloom, N., 1989. Determination of picogram levels of methylmercury by aqueous phase ethylation, followed by cryogenic gas chromatography with cold vapour

atomic fluorescence detection. Can J Fish Aquat Sci 46 (7), 1131–1140. https://doi.org/10.1139/f89-147.
[46] Bowman, K.L., Hammerschmidt, C.R., 2011. Extraction of monomethylmercury from seawater for low-femtomolar determination. Limnol Oceano: Methods 9 (4), 121–128. https://doi.org/10.4319/lom.2011.9.121.
[47] Guédron, S., Duwig, C., Prado, B.L., Point, D., Flores, M.G., Siebe, C., 2014. Methyl) mercury, arsenic, and lead contamination of the world's largest wastewater irrigation system: The Mezquital Valley (Hidalgo State—Mexico). Water, Air, Soil Pollut 225 (8), 2045. https://doi.org/10.1007/s11270-014-2045-3.
[48] Rodriguez-Gonzalez, P., Bouchet, S., Monperrus, M., Tessier, E., Amouroux, D., 2013. In situ experiments for element species-specific environmental reactivity of tin and mercury compounds using isotopic tracers and multiple linear regression. Environ Sci Pollut Res 20 (3), 1269–1280. https://doi.org/10.1007/s11356-012-1019-5.
[49] Maia, R., Eliason, C.M., Bitton, P.-P., Doucet, S.M., Shawkey, M.D., 2013. pavo: An R package for the analysis, visualization and organization of spectral data. Methods Ecol Evol 4, 906–913. https://doi.org/10.1111/2041-210X.12069.
[50] Pucher, M., Wünsch, U., Weigelhofer, G., Murphy, K., Hein, T., Graeber, D., 2019. staRdom: versatile software for analyzing spectroscopic data of dissolved organic matter in R. Water 11 (11), 2366. https://doi.org/10.3390/w11112366.
[51] Lawaetz, A.J., Stedmon, C.A., 2009. Fluorescence intensity calibration using the Raman scatter peak of water. Appl Spectrosc 63 (8), 936–940. https://doi.org/10.1366/000370209788964548.
[52] Kothawala, D.N., Murphy, K.R., Stedmon, C.A., Weyhenmeyer, G.A., Tranvik, L.J., 2013. Inner filter correction of dissolved organic matter fluorescence: correction of inner filter effects. Limnol Oceano: Methods 11 (12), 616–630. https://doi.org/10.4319/lom.2013.11.616.
[53] Coble, P.G., 1996. Characterization of marine and terrestrial DOM in seawater using excitation-emission matrix spectroscopy. Mar Chem 51 (4), 325–346. https://doi.org/10.1016/0304-4203(95)00062-3.
[54] Huguet, A., Vacher, L., Relexans, S., Saubusse, S., Froidefond, J.M., Parlanti, E., 2009. Properties of fluorescent dissolved organic matter in the Gironde Estuary. Org Geochem 40 (6), 706–719. https://doi.org/10.1016/j.orggeochem.2009.03.002.
[55] McKnight, D.M., Boyer, E.W., Westerhoff, P.K., Doran, P.T., Kulbe, T., Andersen, D. T., 2001. Spectrofluorometric characterization of dissolved organic matter for indication of precursor organic material and aromaticity. Limnol Oceanogr 46 (1), 38–48. https://doi.org/10.4319/lo.2001.46.1.0038.
[56] Ohno, T., 2002. Fluorescence inner-filtering correction for determining the humification index of dissolved organic matter. Environ Sci Technol 36 (4), 742–746. https://doi.org/10.1021/es0155276.
[57] R Core Team. (2023). R: A language and environment for statistical computing. [R]. R Foundation for Statistical Computing, Vienna, Austria. ⟨http://www.R-project.org/⟩.
[58] Wickham, H., 2016. ggplot2: Elegant Graphics for Data Analysis. Springer-Verlag, New York. ⟨https://ggplot2.tidyverse.org⟩.
[59] Auguie, B. (2015). gridExtra: Miscellaneous functions for "Grid" graphics. R package version 2.0.0. [Software]. ⟨http://CRAN.R-project.org/package=gridExtra⟩.
[60] Meyers, P.A., 1994. Preservation of elemental and isotopic source identification of sedimentary organic matter. Chem Geol 114 (3-4), 289–302. https://doi.org/10.1016/0009-2541(94)90059-0.
[61] Talbot, M.R., Livingstone, D.A., 1989. Hydrogen index and carbon isotopes of lacustrine organic matter as lake level indicators. Palaeogeogr, Palaeoclimatol, Palaeoecol 70 (1-3), 121–137. https://doi.org/10.1016/0031-0182(89)90084-9.
[62] Gan, S., Schmidt, F., Heuer, V.B., Goldhammer, T., Witt, M., Hinrichs, K.-U., 2020. Impacts of redox conditions on dissolved organic matter (DOM) quality in marine sediments off the River Rhône, Western Mediterranean Sea. Geochim Et Cosmochim Acta 276, 151–169. https://doi.org/10.1016/j.gca.2020.02.001.
[63] Skyllberg, U., Bloom, P.R., Qian, J., Lin, C.-M., Bleam, W.F., 2006. Complexation of mercury(II) in soil organic matter: EXAFS evidence for linear two-coordination with reduced sulfur groups. Environ Sci Technol 40 (13), 4174–4180. https://doi.org/10.1021/es0600577.
[64] Bravo, A.G., Peura, S., Buck, M., Ahmed, O., Mateos-Rivera, A., Herrero Ortega, S., et al., 2018. Methanogens and iron-reducing bacteria: the overlooked members of mercury-methylating microbial communities in Boreal Lakes. Appl Environ Microbiol 84 (23), e01774-18. https://doi.org/10.1128/AEM.01774-18.
[65] Schartup, A.T., Ndu, U., Balcom, P.H., Mason, R.P., Sunderland, E.M., 2015. Contrasting effects of marine and terrestrially derived dissolved organic matter on mercury speciation and bioavailability in seawater. Environ Sci Technol 49 (10), 5965–5972. https://doi.org/10.1021/es506274x.
[66] Taylor, V.F., Buckman, K.L., Seelen, E.A., Mazrui, N.M., Balcom, P.H., Mason, R.P., et al., 2019. Organic carbon content drives methylmercury levels in the water column and in estuarine food webs across latitudes in the Northeast United States. Environ Pollut 246, 639–649. https://doi.org/10.1016/j.envpol.2018.12.064.
[67] Lønborg, C., Álvarez-Salgado, X.A., Davidson, K., Martínez-García, S., Teira, E., 2010. Assessing the microbial bioavailability and degradation rate constants of dissolved organic matter by fluorescence spectroscopy in the coastal upwelling system of the Ría de Vigo. Mar Chem 119 (1), 121–129. https://doi.org/10.1016/j.marchem.2010.02.001.
[68] Romera-Castillo, C., Sarmento, H., Álvarez-Salgado, X.A., Gasol, J.M., Marrasé, C., 2011. Net production and consumption of fluorescent colored dissolved organic matter by natural bacterial assemblages growing on marine phytoplankton exudates. Appl Environ Microbiol 77 (21), 7490–7498. https://doi.org/10.1128/AEM.00200-11.
[69] Bravo, A.G., Kothawala, D.N., Attermeyer, K., Tessier, E., Bodmer, P., Ledesma, J.L. J., et al., 2018. The interplay between total mercury, methylmercury and dissolved organic matter in fluvial systems: a latitudinal study across Europe. Water Res 144, 172–182. https://doi.org/10.1016/j.watres.2018.06.064.
[70] Bouchet, S., Amouroux, D., Rodriguez-Gonzalez, P., Tessier, E., Monperrus, M., Thouzeau, G., et al., 2013. MMHg production and export from intertidal sediments to the water column of a tidal lagoon (Arcachon Bay, France). Biogeochemistry 114 (1-3), 341–358. https://doi.org/10.1007/s10533-012-9815-z.
[71] Bratkič, A., Koron, N., Ribeiro Guevara, S., Faganeli, J., Horvat, M., 2017. Seasonal variation of mercury methylation potential in pristine coastal marine sediment from the Gulf of Trieste (Northern Adriatic Sea). Geomicrobiol J 34 (7), 587–595. https://doi.org/10.1080/01490451.2016.1247482.
[72] Han, S., Obraztsova, A., Pretto, P., Choe, K.-Y., Gieskes, J., Deheyn, D.D., et al., 2007. Biogeochemical factors affecting mercury methylation in sediments of the Venice Lagoon, Italy. Environ Toxicol Chem 26 (4), 655. https://doi.org/10.1897/06-392R.1.
[73] Cesário, R., Hintelmann, H., Mendes, R., Eckey, K., Dimock, B., Araújo, B., et al., 2017. Evaluation of mercury methylation and methylmercury demethylation rates in vegetated and non-vegetated saltmarsh sediments from two Portuguese estuaries. Environ Pollut 226, 297–307. https://doi.org/10.1016/j.envpol.2017.03.075.
[74] Giani, M., Rampazzo, F., Berto, D., Maggi, C., Mao, A., Horvat, M., et al., 2012. Bioaccumulation of mercury in reared and wild *Ruditapes philippinarum* of a Mediterranean lagoon. Estuar, Coast Shelf Sci 113, 116–125. https://doi.org/10.1016/j.ecss.2012.05.031.
[75] French, T.D., Houben, A.J., Desforges, J.-P.W., Kimpe, L.E., Kokelj, S.V., Poulain, A.J., et al., 2014. Dissolved organic carbon thresholds affect mercury bioaccumulation in Arctic lakes. Environ Sci Technol 48 (6), 3162–3168. https://doi.org/10.1021/es403849d.
[76] Rova, S., Stocco, A., Pranovi, F., 2023. Sustainability threshold for multiple ecosystem services in the Venice lagoon, Italy. Ecosyst Serv 64–101568. https://doi.org/10.1016/j.ecoser.2023.101568.